Archives of Hydro-Engineering and Environmental Mechanics
Vol. 54 (2007), No. 2, pp. 117–136

Numerical Simulation of One-Dimensional Two-Phase Flow in Porous Media

Adam Szymkiewicz

Institute of Hydro-Engineering, Polish Academy of Sciences, ul. Kościerska 7,
80-328 Gdańsk, Poland, e-mail: adams@ibwpan.gda.pl

(Received July 13, 2006; revised August 07, 2007)

Abstract

The flow of two immiscible fluids in porous media is described by two coupled non-linear partial differential equations of the parabolic type. In this paper a numerical algorithm to simulate one-dimensional two-phase flow is presented. Cell-centered finite volume method and a generalized two-level scheme with weighting parameter are applied for the discretization in space and time, respectively. The performance of the algorithm is tested for different values of the weighting parameter in the time-discretization scheme and for various methods of approximation of the average conductivities between two adjacent gridblocks. The results are compared with an analytical solution for the horizontal flow and with a reference numerical solution performed on a dense grid for the vertical flow.

Key words: two-phase flow, porous media, numerical methods

1. Introduction

Simultaneous flow of two fluid phases in porous media is a highly non-linear process due to the complex relations between the capillary pressure, phase saturations and conductivities. Typical examples of two-phase flow include oil recovery by water-flooding process in petroleum engineering, flow of water and air in the unsaturated zone of soil or groundwater contamination by non-aqueous phase liquids (NAPL). Various types of mathematical formulation can be used to describe these processes, depending on the relative importance of the forces driving the flow (viscous, capillary and gravitational) and on the compressibility of the two fluid phases. For example, in petroleum engineering a model formulated in terms of the global pressure and fractional flow (Chavent and Jaffre 1987), which was originally developed by neglecting capillary forces and compressibility is often used. It consists of a hyperbolic equation for the saturation and an elliptic equation for the global pressure. Although this model has been extended to cover the case of compressible, capillary-driven flow, it is not necessarily the preferred choice for the

unsaturated zone application, due to its overall complexity and difficulty in implementing general boundary conditions (Binning and Celia 1999). On the other hand, in the unsaturated zone flow models it is routinely assumed that the air phase is at constant, atmospheric pressure. In this way the model is reduced to a single equation for the water phase, known as the Richards equation (Richards 1931). While such an approach is sufficient for many practical applications, a full description of the coupled air and water flow is necessary in some situations, for example when modeling migration of volatile pollutants or rapid infiltration (Touma and Vauclin 1986, Binning 1994, Tegnander 2001). Usually in such cases a two-phase model in the form of two coupled parabolic equations is applied (Touma and Vauclin 1986, Celia and Binning 1992, Kees and Miller 2002).

Numerical methods are the primary tool in unsaturated and two-phase flow modeling. Despite a large body of available literature, the development and improvement of the numerical schemes is still a subject of intensive research. This paper presents a numerical algorithm for one-dimensional flow of two compressible fluid phases using the state-of-the-art techniques. They include a mass-conservative formulation, cell-centered finite volume method for spatial discretization, generalized two-level scheme for the time discretization, adaptive time stepping and the modified Picard method for the solution of the non-linear discretized equations. The accuracy of the scheme is examined on two test problems, concerning horizontal and vertical flow respectively. In particular, we investigate how the overall efficiency of the proposed algorithm is affected by the choice of the weighting parameter in the time discretization scheme and by the method of evaluation of the average conductivities between adjacent gridblocks.

2. Governing Equations

Let us consider isothermal flow of two immiscible liquid phases in a rigid porous medium. The mass conservation principle for each of the two phases can be written in the following form (e.g. Bear 1972, Helmig 1997):

$$\frac{\partial}{\partial t}\left(\rho_\alpha \theta_\alpha\right) + \nabla \cdot \mathbf{q}_\alpha = 0, \tag{1}$$

where: α – phase index ($\alpha = w$ for the wetting phase, e.g. water, and $\alpha = n$ for the non-wetting phase, e.g. air), ρ_α – density of phase α, θ_α – volumetric content of phase α with respect to the bulk volume of the porous medium and $\mathbf{q}_\alpha$ – mass flux of phase α, defined according to the generalized Darcy's law (e.g. Bear 1972, Helmig 1997):

$$\mathbf{q}_\alpha = -\frac{\rho_\alpha}{\mu_\alpha} \kappa k_{r\alpha} \left(\nabla p_\alpha - \rho_\alpha \mathbf{g}\right), \tag{2}$$

where: μ_α – dynamic viscosity coefficient of phase α, κ – absolute permeability of the porous medium, $k_{r\alpha}$ – relative permeability with respect to phase α, p_α – pressure in phase α, and $\mathbf{g}$ – the gravitational acceleration vector. The pore space is entirely occupied by the two phases which implies:

$$\theta_w + \theta_n = \phi, \tag{3}$$

where: ϕ - porosity of the medium. The effective saturation of the wetting phase can be defined as:

$$S_e = \frac{\theta_w - \theta_{rw}}{\phi - \theta_{rn} - \theta_{rw}}, \tag{4}$$

where θ_{rw} and θ_{rn} denote the residual (irreducible) content of each phase. Due to the capillary forces the pressure in the wetting phase (which tends to adhere to the solid surface) is lower than in the non-wetting phase. The difference is defined as the capillary pressure p_c:

$$p_c = p_n - p_w. \tag{5}$$

The relations between the capillary pressure, effective wetting phase saturation and phase permeabilities are given by a set of constitutive functions. The two most popular constitutive models are the Brooks – Corey – Burdine model (Brooks and Corey 1964, Burdine 1953):

$$S_e = \left(\frac{p_c}{p_e}\right)^{-\lambda} \text{ for } p_c > p_e; \quad S_e = 1 \text{ for } p_c \le p_e, \tag{6}$$

$$k_{rw} = S_e^{(3+2/\lambda)}, \tag{7}$$

$$k_{rn} = (1 - S_e)^2 \left(1 - S_e^{(1+2/\lambda)}\right) \tag{8}$$

and the van Genuchten – Mualem model (van Genuchten 1980, Mualem 1976):

$$S_e = \left[1 + \left(\frac{p_c}{p_e}\right)^n\right]^{-m}, \tag{9}$$

$$k_{rw} = \sqrt{S_e}\left[1 - \left(1 - S_e^{1/m}\right)^m\right]^2, \tag{10}$$

$$k_{rn} = \sqrt{1 - S_e}\left(1 - S_e^{1/m}\right)^{2m}. \tag{11}$$

In the Brooks – Corey – Burdine model p_e corresponds to the non-wetting phase entry pressure, while in the van Genuchten – Mualem model it is a scaling

parameter with no direct physical interpretation. The exponents λ, n and $m = 1 - 1/n$ are related to the texture of the considered porous medium.

Finally, a relation between the density and pressure of each phase should be specified. For the water it can be assumed that (e.g. Kees and Miller 2002):

$$\rho_w (p_w) = \rho_{w,0} \exp (a (p_w - p_{w,0})), \tag{12}$$

where a is the water compressibility coefficient and $\rho_{w,0}$ and $p_{w,0}$ denote the reference density and pressure. For the air phase one can use the ideal gas law (e.g. Kees and Miller 2002):

$$\rho_n (p_n) = \rho_{n,0} + \frac{M_m}{RT} (p_n - p_{n,0}) = \rho_{n,0} + b (p_n - p_{n,0}), \tag{13}$$

where: M_m – mole mass of the air, R – gas constant, T – absolute temperature and b – air compressibility coefficient. In soil hydrology it is more convenient to use the pressure head instead of the pressure and to relate it to the atmospheric pressure head. The following substitution of variables is introduced (e.g. Kees and Miller 2002):

$$\hat{\rho}_a = \frac{\rho_\alpha}{\rho_{w,0}}, \quad \hat{\mu}_\alpha = \frac{\mu_w}{\mu_\alpha}, \quad \psi_\alpha = \frac{p_\alpha - p_{atm}}{\rho_{w,0} \|\mathbf{g}\|}, \quad K_S = \frac{\rho_{w,0} \|\mathbf{g}\| \kappa}{\mu_w}, \quad K_\alpha = \hat{\rho}_a \hat{\mu}_\alpha K_S k_{r\alpha}, \tag{14}$$

where: ψ_α – pressure head in phase α, p_{atm} – atmospheric pressure, K_α – hydraulic conductivity of the phase α, K_s – conductivity of the wetting phase at full saturation and $\|\mathbf{g}\|$ – norm of the gravitational vector. Using the above variables, the one-dimensional form of Eq. (1) can be written as follows:

$$\frac{\partial}{\partial t} (\hat{\rho}_\alpha \theta_\alpha) - \frac{\partial}{\partial x} \left(K_\alpha \left(\frac{\partial \psi_\alpha}{\partial x} - \gamma \hat{\rho}_\alpha \right) \right) = 0, \tag{15}$$

where $\gamma = 1$ for vertical flow and $\gamma = 0$ for horizontal flow.

3. Discrete Formulation

3.1. Choice of the Primary Variables

The first step in the formulation of the numerical scheme is to choose which variables should be the primary ones. One possibility is to choose the two pressure heads, ψ_w and ψ_n (e.g. Celia and Binning 1992). In this case we obtain two equations analogous to the Richards equation in the pressure-based form, which is well-known in the literature (e.g. Zaradny 1993). However, if the non-wetting phase disappears the corresponding equation becomes singular. In order to overcome this problem, a mixed pressure – saturation (or pressure – phase content) formulation is recommended (Helmig 1997). Of the four possible combinations $\psi - \theta$ we choose the

wetting phase pressure head ψ_w and the wetting phase volumetric content θ_w as the primary variables.

3.2. Spatial Discretization

The governing equations are discretized in space with a cell-centered finite volume method, which is widely used for flow and transport problems (e.g. Chavent et al 1997, Morton 1996). The solution domain is divided into N gridblocks (finite volumes), which can have different dimensions. The unknowns are positioned in the geometric centers of the gridblocks and are assumed to represent the mean values of the respective variables in the considered gridblock. For any gridblock i one can write the mass conservation principle in the discrete form:

$$V_i \frac{\partial}{\partial t}(\hat{\rho}_\alpha \theta_\alpha) - S_{i-1/2} q_{\alpha,i-1/2} + S_{i+1/2} q_{\alpha,i+1/2} = 0, \tag{16}$$

where V_i is the volume of the gridblock, $S_{i+1/2}$ and $S_{i-1/2}$ denote the area of the interface between the cells and $q_{\alpha,i+1/2}$ and $q_{\alpha,i-1/2}$ the respective mass fluxes of each phase. For one-dimensional flow in cartesian coordinates, we have $S_{i\pm1/2} = 1$ = const and $V_i = \Delta L_i$, where ΔL_i is the length of the gridblock. Extension for the case of radial flow is straightforward. The fluxes at the cell interfaces are given by the following expressions:

$$q_{w,i+1/2} = -\bar{K}_{w,i+1/2}\left(\frac{\psi_{w,i+1} - \psi_{w,i}}{\Delta x_{i+1/2}} - \gamma \frac{\hat{\rho}_{w,i+1} + \hat{\rho}_{w,i}}{2}\right) \tag{17}$$

and:

$$q_{n,i+1/2} = -\bar{K}_{n,i+1/2}\left(\frac{\psi_{w,i+1} - \psi_{w,i}}{\Delta x_{i+1/2}} + \frac{\psi_c(\theta_{w,i+1}) - \psi_c(\theta_{w,i})}{\Delta x_{i+1/2}} - \gamma \frac{\hat{\rho}_{n,i+1} + \hat{\rho}_{n,i}}{2}\right), \tag{18}$$

where $\bar{K}_{\alpha,i+1/2}$ denote the interblock conductivities of each phase, which are discussed in more detail below and $\Delta x_{i+1/2} = 0.5(\Delta L_i + \Delta L_{i+1})$ is the distance between the centers of the adjacent gridblocks.

For the first and the last cell, the scheme has to be modified to account for the imposed boundary conditions. Consider, for example, the last gridblock. For Dirichlet boundary conditions we replace $\psi_{w,i+1}$ and $\theta_{w,i+1/2}$ in Eqs. (17) and (18) with the values specified at the boundary, while $\Delta x_{i+1/2}$ is set equal to $0.5\Delta L_N$. For Neumann boundary conditions we replace $q_{\alpha,i+1/2}$ with the mass fluxes specified at the boundary.

3.3. Approximation of the Interblock Conductivites

The overall accuracy of the numerical solution depends significantly on the method of estimation of the inter-block conductivities. This problem has been investigated by many researchers for the case of one-dimensional Richards equation (e.g. Haverkamp and Vauclin 1979, Belfort and Lehmann 2005), but relatively less attention has been paid to the full two-phase model (Helmig and Huber 1998). In this paper five averaging methods, originally proposed for the Richards equation, are used in the two-phase flow simulations. They include:

- arithmetic mean (e.g. Celia and Binning 1992, Kees and Miller 2002):

$$\bar{K}_{\alpha,i+1/2} = \frac{1}{2}\left(K_{\alpha,i} + K_{\alpha,i+1}\right), \tag{19}$$

- geometric mean (e.g. Haverkamp and Vauclin 1979):

$$\bar{K}_{\alpha,i+1/2} = \sqrt{K_{\alpha,i} K_{\alpha,i+1}}, \tag{20}$$

- harmonic mean (e.g. Manzini and Ferraris 2004):

$$\bar{K}_{\alpha,i+1/2} = \frac{2K_{\alpha,i} K_{\alpha,i+1}}{K_{\alpha,i} + K_{\alpha,i+1}}, \tag{21}$$

- upstream weighting (e.g. Helmig 1997):

$$\bar{K}_{\alpha,i+1/2} = K_{\alpha,i} \text{ if } \left(\frac{\partial \psi_\alpha}{\partial x} - \gamma \hat{\rho}_\alpha\right) \leq 0, \tag{22a}$$

$$\bar{K}_{\alpha,i+1/2} = K_{\alpha,i+1} \text{ if } \left(\frac{\partial \psi_\alpha}{\partial x} - \gamma \hat{\rho}_\alpha\right) > 0, \tag{22b}$$

- integral mean (e.g. Baker 2000):

$$\bar{K}_{\alpha,i+1/2} = \kappa \hat{\mu}_\alpha \frac{\left(\hat{\rho}_{\alpha,i} + \hat{\rho}_{\alpha,i+1}\right)}{2} \frac{1}{\left|\psi_{c,i+1} - \psi_{c,i}\right|} \int_{\psi_{c,i}}^{\psi_{c,i+1}} k_{r\alpha}\left(\psi_c\right) d\psi_c. \tag{23}$$

The integral in Eq. (23) can be computed analytically for the Brooks – Corey – Burdine model or approximated by an analytical expression for the van Genuchten model. However, in our implementation the integral is evaluated numerically using 16 internal points in the interval $< \psi_{c,i};\ \psi_{c,i+1} >$, which represents a more general approach, suitable for any type of constitutive functions.

3.4. Integration in Time

From the spatial discretization one obtains a system of $2 \times N$ ordinary differential equations with respect to time. The system has to be integrated in the specified time interval $< 0; t_{final} >$. In this work a generalized two-level time integration scheme with a weighting parameter is used. It can be written in the following form:

$$(\hat{\rho}_\alpha \theta_\alpha)_i^{j+1} = (\hat{\rho}_\alpha \theta_\alpha)_i^j + \Delta t^{j+1} \left[(1-\omega) \left. \frac{\partial (\hat{\rho}_\alpha \theta_\alpha)}{\partial t} \right|_i^j + \omega \left. \frac{\partial (\hat{\rho}_\alpha \theta_\alpha)}{\partial t} \right|_i^{j+1} \right], \tag{24}$$

where j is the index of the time level and ω the weighting parameter. In order to ensure mass conservation the entire mass term $(\rho_\alpha \theta_\alpha)$ is discretized, instead of introducing the time derivatives of the primary variables (Celia et al 1990, Kees and Miller 2002). Eq. (24) represents the fully implicit (implicit Euler) scheme for $\omega = 1$ and the Crank-Nicholson scheme for $\omega = 0.5$. Stability analysis for the linear case indicates that the scheme is absolutely stable for $\omega \geq 0.5$. For the highly non-linear Richards equation $\omega \geq 0.57$ was recommended (Narasimhan et al 1978, cited after Zaradny 1993). The same authors proposed a method for adjusting ω during the solution, in order to optimize the performance of the scheme. Nevertheless, most of the algorithms for two-phase and unsaturated flow available in the literature use the fully implicit approach with $\omega = 1$ (e.g. Celia et al 1990). Recently Kees and Miller (2002) proposed to use sophisticated variable-order methods for the integration in time, of the two-phase flow equations. Despite the possible advantages, this approach is not considered here, since it increases significantly the overall complexity of the algorithm.

Application of the scheme (24) to the semi-discrete form of the governing equations, given by Eq. (16), yields a system of non-linear algebraic equations of the form:

$$\mathbf{R}\left(\mathbf{u}^{j+1}\right) = \mathbf{0}, \tag{25}$$

where $\mathbf{R}$ is a vector of $2{\times}N$ nodal residual values, $\mathbf{R} = (R_{w,1}, R_{n,1}, R_{w,2}, R_{n,2}, \ldots, R_{w,N}, R_{n,N})^{\mathrm{T}}$. The odd components of $\mathbf{R}$ are defined by Eq. (26) and the even components defined by Eq. (27) below:

$$\begin{aligned} R_{w,i} \equiv\; & V_i \, (\hat{\rho}_w \theta_w)_i^{j+1} - V_i \, (\hat{\rho}_w \theta_w)_i^j - \Delta t^{j+1} \, (1-\omega) \, V_i \left. \frac{\partial (\hat{\rho}_w \theta_w)}{\partial t} \right|_i^j + \\ & - \Delta t^{j+1} \omega \left[\bar{K}_{w,i-1/2}^{j+1} \left(\frac{\psi_{w,i}^{j+1} - \psi_{w,i-1}^{j+1}}{\Delta x_{i-1/2}} - \gamma \frac{\hat{\rho}_{w,i}^{j+1} + \hat{\rho}_{w,i-1}^{j+1}}{2} \right) + \right. \\ & \left. - \bar{K}_{w,i+1/2}^{j+1} \left(\frac{\psi_{w,i+1}^{j+1} - \psi_{w,i}^{j+1}}{\Delta x_{i+1/2}} - \gamma \frac{\hat{\rho}_{w,i+1}^{j+1} + \hat{\rho}_{w,i}^{j+1}}{2} \right) \right] = 0, \end{aligned} \tag{26}$$

$$R_{n,i} \equiv V_i \left(\hat{\rho}_n \theta_n\right)_i^{j+1} - V_i \left(\hat{\rho}_n \theta_n\right)_i^{j} - \Delta t^{j+1} \left(1-\omega\right) V_i \left.\frac{\partial \left(\hat{\rho}_n \theta_n\right)}{\partial t}\right|_i^j +$$
$$-\Delta t^{j+1} \omega \left[\bar{K}_{n,i-1/2}^{j+1} \left(\frac{\psi_{w,i}^{j+1} - \psi_{w,i-1}^{j+1}}{\Delta x_{i-1/s}} + \frac{\psi_c\left(\theta_{w,i}^{j+1}\right) - \psi_c\left(\theta_{w,i-1}^{j+1}\right)}{\Delta x_{i-1/2}} - \gamma \frac{\hat{\rho}_{w,i}^{j+1} + \hat{\rho}_{w,i-1}^{j+1}}{2} \right) + \right. \tag{27}$$
$$\left. -\bar{K}_{n,i+1/2}^{j+1} \left(\frac{\psi_{w,i+1}^{j+1} - \psi_{w,i}^{j+1}}{\Delta x_{i+1/s}} + \frac{\psi_c\left(\theta_{w,i+1}^{j+1}\right) - \psi_c\left(\theta_{w,i}^{j+1}\right)}{\Delta x_{i+1/2}} - \gamma \frac{\hat{\rho}_{n,i+1}^{j+1} + \hat{\rho}_{n,i}^{j+1}}{2} \right) \right] = 0.$$

The vector $\mathbf{u}^{j+1}$ is composed of the nodal values of the unknowns θ_w and ψ_w, $\mathbf{u}^{j+1} = (\theta_{w,1}, \psi_{w,1} \ldots, \theta_{w,N}, \psi_{w,N})^T$. The time derivatives at the time level $j = 0$ are computed via Eq. (16) from the initial condition. The system of equations (25) resulting for each time step is highly non-linear and has to be solved by an iterative approach.

3.5. Iterative Solution

At each time level t^j the solution of Eq. (25) starts with some initial approximation $\mathbf{u}$. In this work we use the solution from the previous time level:

$$u_i^{j+1,0} = u_i^j. \tag{28}$$

The approximate solution $\mathbf{u}$ is corrected in subsequent iterations according to the formula:

$$u_i^{j+1,k+1} = u_i^{j+1,k} + \delta u_i^{j+1,k+1}, \tag{29}$$

where k is the iteration index and $\delta \mathbf{u}^{\,j+1,k+1} = (\delta\theta_{w,1}, \delta\psi_{w,1}, \ldots \delta\theta_{w,N}, \delta\psi_{w,N})^{\mathrm{T}}$ is the increment (correction) vector, which is computed from the following system of equations:

$$\mathbf{J}^{j+1,k} \delta \mathbf{u}^{j+1,k+1} = -\mathbf{R}^{j+1,k}. \tag{30}$$

The form of the matrix $\mathbf{J}$ depends on the chosen iterative scheme. For the standard Newton method, it represents the jacobian of $\mathbf{R}$, i.e. $J_{pq} = (\partial R_p / \partial u_q)$. The evaluation of the partial derivatives can be computationally costly. Thus we used another approach known as the modified Picard method (Celia et al 1990, Binning 1994), where $\mathbf{J}$ is only an approximation of the jacobian. For any internal node i Eq. (30) gives the following two linearized equations:

$$V_i \rho_{n,i}^{j+1,k} \delta\theta_{w,i}^{j+1,k+1} +$$

$$+\left[V_i \theta_{w,i}^{j+1,k} \left(\frac{d\hat{\rho}_w}{d\psi_w} \right)_i^{j+1,k} + \Delta t^{j+1} \omega \left(\frac{\bar{K}_{w,i-1/2}^{j+1,k}}{\Delta x_{i-1/2}} + \frac{\bar{K}_{w,i+1/2}^{j+1,k}}{\Delta x_{i+1/2}} \right) \right] \delta\psi_{w,i}^{j+1,k+1} + \tag{31}$$

$$-\Delta t^{j+1} \omega \frac{\bar{K}_{w,i-1/2}^{j+1,k}}{\Delta x_{i-1/2}} \delta\psi_{w,i-1}^{j+1,k+1} - \Delta t^{j+1} \omega \frac{\bar{K}_{w,i+1/2}^{j+1,k}}{\Delta x_{i+1/2}} \delta\psi_{w,i+1}^{j+1,k+1} = -R_{w,i}^{j+1,k},$$

$$V_i \left[\theta_{n,i}^{j+1,k} \left(\frac{d\hat{\rho}_n}{d\psi_n} \frac{d\psi_c}{d\theta_w} \right) \Big|_i^{j+1,k} - \hat{\rho}_{n,i}^{j+1,k} \right] \delta\theta_{w,i}^{j+1,k+1} +$$

$$+\left[V_i \theta_{n,i}^{j+1,k} \left(\frac{d\hat{\rho}_n}{d\psi_n} \right)_i^{j+1,k} + \Delta t^{j+1} \omega \left(\frac{\bar{K}_{n,i-1/2}^{j+1,k}}{\Delta x_{i-1/2}} + \frac{\bar{K}_{n,i+1/2}^{j+1,k}}{\Delta x_{i+1/2}} \right) \right] \delta\psi_{w,i}^{j+1,k+1} + \tag{32}$$

$$-\Delta t^{j+1} \omega \frac{\bar{K}_{n,i-1/2}^{j+1,k}}{\Delta x_{i-1/2}} \delta\psi_{w,i-1}^{j+1,k+1} - \Delta t^{j+1} \omega \frac{\bar{K}_{n,i+1/2}^{j+1,k}}{\Delta x_{i+1/2}} \delta\psi_{w,i+1}^{j+1,k+1} = -R_{n,i}^{j+1,k}.$$

The first two terms in each equation result from the application of the chain differentiation rule to calculate the derivatives of the mass term ($\rho_\alpha \theta_\alpha$) with respect to θ_w and ψ_w. Since the discrete form of the equation at node i is based on the values of the θ_w and ψ_w at nodes i, $i-1$ and $i+1$, the matrix is banded (with the bandwidth equal to 7) and consequently the system (30) can be effectively solved by a direct method (Szmelter 1980). New approximations of the unknowns are then calculated from Eq. (29). The iterative process is stopped when the local mass balance error for each gridblock is smaller than the prescribed value:

$$R_{w,i} \leq err_{w,i}, \quad R_{n,i} \leq err_{n,i}. \tag{33}$$

The allowable errors are defined as:

$$err_{\alpha,i} = \varepsilon_{MB} V_i \rho_{\alpha,i}, \tag{34}$$

where ε_{MB} is a user-specified tolerance coefficient. The allowable mass balance error is related to the maximum possible amount of mass of the given phase in the gridblock. It is independent of the actual amount of mass, which may be equal to zero in some conditions. While other types of termination criteria can be used as well (e.g. Zaradny 1993), preliminary tests showed that the mass balance criterion is efficient for the range of numerical examples presented in this work. Moreover, it is directly related to the physical interpretation of the governing equations.

3.6. Time-Stepping Scheme

In order to improve the efficiency of the numerical scheme the time-step size should be adjusted during the solution. When large pressure gradients are imposed at the

boundaries the solution starts with small time steps, which are increased later, as the solution becomes smoother. In our algorithm, we used a simple time stepping scheme, which adjusts the step in such a way that the number of iterations at each time level is kept in a prescribed range.

- if the number of iterations is lower than 3, then $\Delta t^{j+1} = 1.1\ \Delta t^{j}$,
- if the number of iterations is higher than 7, then $\Delta t^{j+1} = 0.56\ \Delta t^{j}$,
- if the solution did not converge after 21 iterations, then restart the calculations for the current time level reducing the Δt by 4.

The choice of the coefficients is empirical. Although more sophisticated methods of time-stepping are available (Kees and Miller 2002, Kavetski et al 2001), we found that this simple scheme performed well for all simulations presented in this paper.

4. Numerical Examples

4.1. Example 1

The first problem concerns horizontal flow of two incompressible fluids. The properties of the two fluids correspond to those of air and water, except for the compressibility, which is set equal to zero, in order to compare the results with the semi-analytical solution. The parameters for this problem are listed in Table 1. The solution is carried out for a spatial domain of the length $L = 0.8$ m and for time up to 3000 s. The initial wetting phase (water) content is $\theta_w = 0.003$, which

Table 1. Parameters of the test problems

Parameter	Example 1	Example 2
L [m]	0.8	0.8
t_{final} [s]	3000	5500
γ [–]	0	1
$\rho_{w,0}$ [kg s^{-1}]	1000	1000
$\rho_{n,0}$ [kg s^{-1}]	1.204	1.204
a [Pa^{-1}]	0	4.9×10^{-10}
b [kg m^{-3} Pa^{-1}]	0	1.189×10^{-5}
μ_w [Pa s]	1.0×10^{-3}	1.0×10^{-3}
μ_n [Pa s]	1.57×10^{-5}	1.57×10^{-5}
ϕ [–]	0.3	0.43
θ_{rw} [–]	0	0.045
θ_{rn} [–]	0	0
ψ_e [m]	0.102	0.069
λ [–]	2	–
n [–]	–	2.68
K_s [m s^{-1}]	9.81×10^{-4}	8.25×10^{-5}

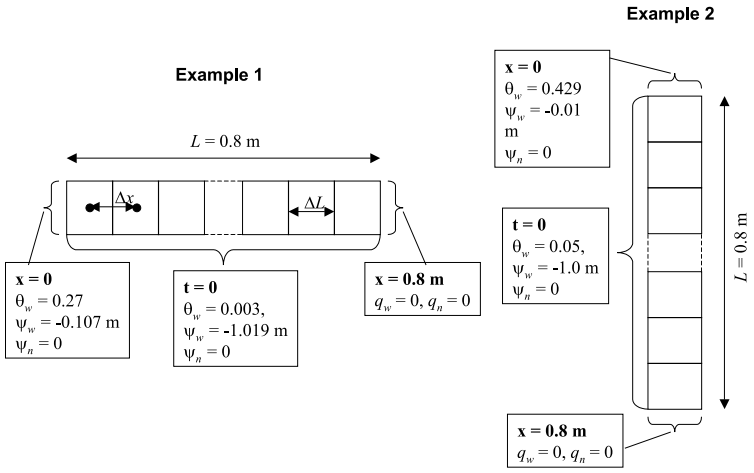

Fig. 1. Solution domain and boundary condition used in the numerical examples

corresponds to the effective saturation $S_e = 0.01$ (Fig. 1). At the left boundary $x = 0$ a constant saturation $S_e = 0.9$ ($\theta_w = 0.27$) is maintained. The other boundary is assumed impermeable for both fluids. A bi-directional displacement occurs, i.e the wetting phase invades the domain from left to right, while at the other time the non-wetting phase leaves the domain by the left boundary. For such setting a semi-analytical solution of Sunada and McWhorter (1990) can be applied. The details of the implementation of the semi-analytical solution are discussed in the work of Fučik (2006). The time of the flow was chosen in such a manner that the right-hand side boundary (which in the analytical solution is assumed at $x = \infty$) does not influence the simulated process. Two series of calculations were performed. In the first series we compare the results for different values of ω and for different numbers of gridblocks N, ranging from 10 to 80. The interblock conductivities were approximated as arithmetic means. The mass balance tolerance coefficient in Eq. (34), ε_{MB}, was set equal to 10^{-6} (the same value was used in all simulations presented in this paper). The results are summarized in Table 2. The accuracy of the scheme is measured in terms of the error in the cumulative amount of infiltrated water *TMerr*:

$$TMerr = \left(\frac{TMnum}{TMref} - 1 \right) \cdot 100\%, \tag{35}$$

where $TMnum$ is the total mass of water that entered the domain at $x = 0$ computed from the numerical solution and $TMref$ is the corresponding value given by the analytical solution. The values of $TMerr$ are reported in Table 2. Other parameters listed in Table 2 include the mass balance error for each phase, number of time steps, number of iterations and the real time of the calculations. The number of iterations represents the sum of iterations performed for all time steps, i.e. it shows

Table 2. Example 1: Numerical results for different numbers of gridblocks (N) and time-integration coefficients ω

N	ω [–]	$TMerr$ [%]	$MBerr_w$ [%]	$MBerr_n$ [%]	time steps [–]	iterations [–]	time [s]
10	0.5	9.90	1.45×10^{-04}	2.38×10^{-03}	6481	18956	3
	0.57	9.90	7.89×10^{-03}	9.04×10^{-03}	6788	19876	2
	0.667	9.90	1.69×10^{-02}	1.81×10^{-02}	7552	22175	2
	1	10.00	3.85×10^{-02}	3.97×10^{-02}	9826	28991	3
20	0.5	4.42	1.10×10^{-04}	1.66×10^{-03}	14203	42148	6
	0.57	4.42	4.42×10^{-03}	4.98×10^{-03}	15413	45773	7
	0.667	4.42	9.68×10^{-03}	1.03×10^{-02}	17041	50656	7
	1	4.42	2.16×10^{-02}	2.22×10^{-02}	23162	69027	9
40	0.5	1.88	3.90×10^{-05}	8.70×10^{-04}	34109	101875	25
	0.57	1.88	2.40×10^{-03}	2.69×10^{-03}	36730	109752	24
	0.667	1.88	5.12×10^{-03}	5.42×10^{-03}	41379	123700	27
	1	1.88	1.17×10^{-02}	1.20×10^{-02}	53805	160980	35
80	0.5	0.75	5.10×10^{-04}	2.00×10^{-04}	82899	248281	107
	0.57	0.75	1.25×10^{-03}	1.40×10^{-03}	90220	270244	106
	0.667	0.75	2.62×10^{-03}	2.76×10^{-03}	99592	298362	116
	1	0.76	6.23×10^{-03}	6.38×10^{-03}	130251	390347	153

how many times the linear system (31)–(32) was solved during the entire simulation. Comparing the numbers of iterations and time steps, it can be seen that on average about three iterations were performed in each time step. The mass balance error is defined as:

$$MB_\alpha = \frac{\sum_{i=1}^{N} L_i(\rho_\alpha\theta_\alpha)_i^{t_{final}} - \sum_{i=1}^{N} L_i\,(\rho_\alpha\theta_\alpha)_i^{t=0} - \int_{t=0}^{t_{final}} q_\alpha^{(1)}dt + \int_{t=0}^{t_{final}} q_\alpha^{(2)}dt}{\min\left(\left|\sum_{i=1}^{N} L_i\,(\rho_\alpha\theta_\alpha)_i^{t_{final}} - \sum_{i=1}^{N} L_i\,(\rho_\alpha\theta_\alpha)_i^{t=0}\right|, \left|\int_{t=0}^{t=t_{final}} q_\alpha^{(1)}dt - \int_{t=0}^{t=t_{final}} q_\alpha^{(2)}dt\right|\right)} \cdot 100\% \quad (36)$$

where $q_\alpha^{(1)}$ and $q_\alpha^{(2)}$ denote the boundary fluxes at $x = 0$ and $x = L$, respectively. The integrals of the boundary fluxes are calculated from the numerical solution using the trapezoidal rule.

It can be seen that the scheme is convergent, i.e. when Δx is reduced, the cumulative mass error tends to zero. Since doubling the number of gridblocks results in more than 50% error reduction, the overall order of accuracy of the scheme can be estimated as slightly greater than one. The convergence to analytical solution is also visible in Fig. 2, which presents the distribution of the wetting phase content for $t = t_{final} = 3000$ s for various discretizations and $\omega = 0.57$. The $\theta_w(x)$ profiles are virtually the same for all values of the coefficient ω. This is consistent with the fact that the cumulative infiltrated mass (TM_w), representing the area under the profile $\theta_w(x)$ for a given time level, practically does not depend on ω. On the

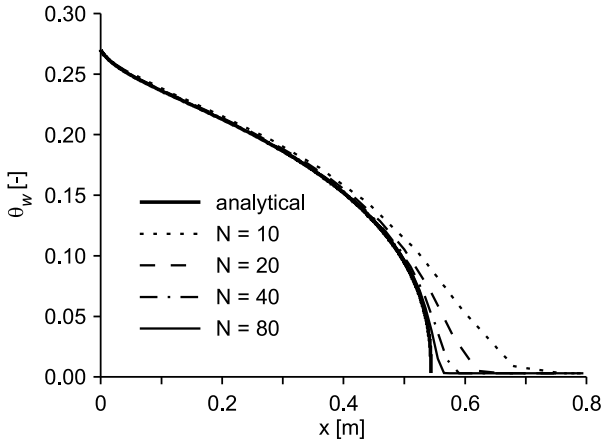

Fig. 2. Example 1: Water content profiles after 3000 s of infiltration obtained with different number of gridblocks, $\omega = 0.57$, arithmetic conductivity averaging

other hand, the choice of ω seems to influence significantly the overall efficiency of the scheme. It can be seen that as ω approaches 0.5 the number of iterations and consequently the CPU time required for the simulation is reduced by about 30%. However, for $\omega = 0.5$ unphysical oscillations were observed in the solution. The wetting and non-wetting pressure heads and fluxes strongly oscillated from one time level to another, while the capillary head remained constant. The oscillations in the instantaneous wetting phase flux q_w at $x = 0$ are shown in Fig. 3. Note that the oscillations disappear for $\omega > 0.5$. This is consistent with the suggestions of Narasimhan et al (1978) (cited after Zaradny (1993)). The mass balance error is very low for all simulations, which results from the applied mass-conservative scheme and from the convergence criterion Eq. (34) enforcing good mass balance in each gridblock.

The second series of tests concerned various methods of evaluation of the interblock conductivity. The results shown in Table 3 were obtained for $\omega = 0.57$, which was chosen as the "optimal" value, based on the first series of tests. In Figs. 4 and 5 we present the $\theta_w(x)$ profiles for the final time $t = 3000$ s obtained using 10 and 40 gridblocks, respectively. It can be seen that various averaging formulae give very different results. Comparison of Figs. 4 and 5 shows that as the number of the gridblocks increases, most of the averaging schemes converge to the reference solution, except for the harmonic mean, which practically does not produce any flow at all.

This latter result is consistent with the simulations presented by Belfort and Lehmann (2005). In fact it is well known that the harmonic mean severely underestimates the interblock conductivities. Nevertheless, it is used in some numerical models available in the literature (e.g. Manzini and Ferraris 2004). Note that the integral mean gives very good results even for the coarse discretization. Again,

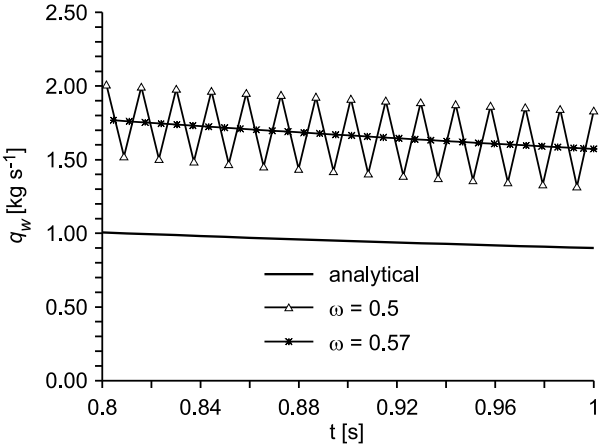

Fig. 3. Example 1: Instantaneous water flux according to the analytical solution and numerical solution with $\omega = 0.5$ and $\omega = 0.57$ ($N = 20$, arithmetic conductivity averaging)

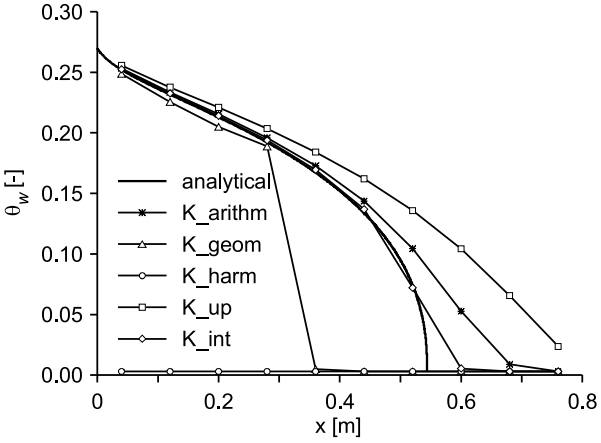

Fig. 4. Example 1: Water content profiles after 3000 s of infiltration obtained with different methods of conductivity averaging, $\omega = 0.57$, $N = 10$

this is consistent with the results of other authors (e.g. Baker 2000). The time of simulation using integral mean is significantly longer than for other formulae (Table 3). This is due to the numerical evaluation of the integral. The computational time can be reduced if exact or approximate analytical expressions for the integrals, available for some types of constitutive functions, are used instead of numerical integration.

Table 3. Example 1: Numerical results for different numbers of gridblocks (N) and conductivity averaging methods

N	averaging scheme	$TMerr$ [%]	$MBerr_w$ [%]	$MBerr_n$ [%]	time steps [–]	iterations [–]	time [s]
10	arithm	9.90	7.89×10^{-03}	9.04×10^{-03}	6788	19876	2
	geom	–30.33	1.66×10^{-04}	3.54×10^{-04}	7171	20975	2
	harm	–100.00	1.65×10^{-03}	5.20×10^{-01}	399	574	0
	up	26.95	5.23×10^{-03}	7.94×10^{-03}	29517	88199	10
	int	1.78	3.85×10^{-03}	5.25×10^{-03}	6843	20024	6
20	arithm	4.42	4.42×10^{-03}	4.98×10^{-03}	15413	45773	7
	geom	–14.97	6.30×10^{-04}	5.39×10^{-04}	18062	53670	7
	harm	–100.00	1.81×10^{-03}	1.94×10^{-01}	608	1224	0
	up	15.89	2.94×10^{-03}	4.33×10^{-03}	72174	216189	31
	int	0.74	2.19×10^{-03}	2.88×10^{-03}	16223	48192	22
40	arithm	1.88	2.40×10^{-03}	2.69×10^{-03}	36730	109752	24
	geom	–6.17	4.74×10^{-04}	4.33×10^{-04}	45510	136038	31
	harm	–99.99	1.99×10^{-03}	3.34×10^{-02}	1506	3958	1
	up	8.99	1.57×10^{-03}	2.32×10^{-03}	155804	467096	107
	int	0.28	1.17×10^{-03}	1.50×10^{-03}	39192	117119	101
80	arithm	0.75	1.25×10^{-03}	1.40×10^{-03}	90220	270244	106
	geom	–2.28	2.58×10^{-04}	2.42×10^{-04}	114170	342050	140
	harm	–99.96	5.05×10^{-03}	1.02×10^{-02}	5812	16895	7
	up	5.03	8.45×10^{-04}	1.24×10^{-03}	277508	832225	339
	int	0.10	6.49×10^{-04}	8.15×10^{-04}	95710	286693	481

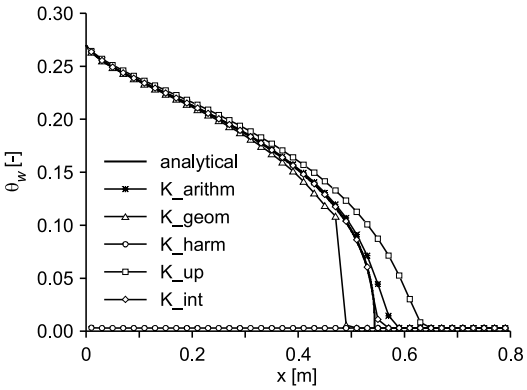

Fig. 5. Example 1: Water content profiles after 3000 s of infiltration obtained with different methods of conductivity averaging, $\omega = 0.57$, $N = 40$

4.2. Example 2

The second test problem concerns vertical infiltration of water into an air-filled column that is sealed at the bottom (Fig. 1). In contrast to the previous example, realistic values of the water and air compressibility were assumed here. Since no analytical solution exists for such case, we used as the reference a numerical solution on a relatively dense grid (640 gridblocks), with arithmetic averaging and $\omega = 0.57$, which is assumed to be close to the exact solution. Similarly to the previous case, the first series of simulations was performed using the arithmetic mean formula for different values of ω and various number of gridblocks. The results are listed in Table 4 and the water content profiles are shown in Fig. 6 for the case of $\omega = 0.57$. Similar relations between ω and the simulation time as in Test problem 1 can be noticed. In this case no oscillations were observed for $\omega = 0.5$.

Table 4. Example 2: Numerical results for different numbers of gridblocks (N) and time--integration coefficients ω

N	ω [–]	$TMerr$ [%]	$MBerr_w$ [%]	$MBerr_n$ [%]	time steps [–]	iterations [–]	time [s]
10	0.5	8.07	4.65×10^{-07}	8.46×10^{-04}	4316	12463	2
	0.57	8.07	4.37×10^{-03}	4.98×10^{-03}	4484	12973	2
	0.667	8.07	9.02×10^{-03}	9.33×10^{-03}	5250	15272	2
	1	8.07	2.15×10^{-02}	2.09×10^{-02}	6749	19773	3
20	0.5	4.66	3.96×10^{-07}	4.59×10^{-04}	9583	28293	5
	0.57	4.66	2.55×10^{-03}	2.85×10^{-03}	10262	30334	5
	0.667	4.66	5.47×10^{-03}	5.58×10^{-03}	11779	34878	6
	1	4.66	1.25×10^{-02}	1.21×10^{-02}	14693	43632	8
40	0.5	2.46	2.53×10^{-07}	2.37×10^{-04}	21866	65162	18
	0.57	2.46	1.41×10^{-03}	1.55×10^{-03}	24302	72476	21
	0.667	2.46	3.05×10^{-03}	3.08×10^{-03}	26486	79028	22
	1	2.46	7.12×10^{-03}	6.85×10^{-03}	35139	104983	29
80	0.5	1.15	1.50×10^{-07}	1.27×10^{-04}	54238	162305	81
	0.57	1.15	7.80×10^{-04}	8.49×10^{-04}	57940	173413	88
	0.667	1.15	1.68×10^{-03}	1.68×10^{-03}	65940	197413	99
	1	1.15	3.96×10^{-03}	3.78×10^{-03}	84025	251671	126

The influence of the conductivity averaging formulae is different for vertical flow than it was for the horizontal flow (Table 5, Figs. 7 and 8). It can be seen that, on average, the best results were obtained for the arithmetic mean, which produced moderate error for coarse discretizations and quickly converged to the reference solution. The integral mean leads to unphysical oscillations for coarse discretization (Fig. 7), while it is the most accurate approximation for small Δx. The geometric mean, recommended by some authors (e.g. Haverkamp and Vauclin 1979) as the best choice for vertical infiltration performs worse than the arithmetic mean in

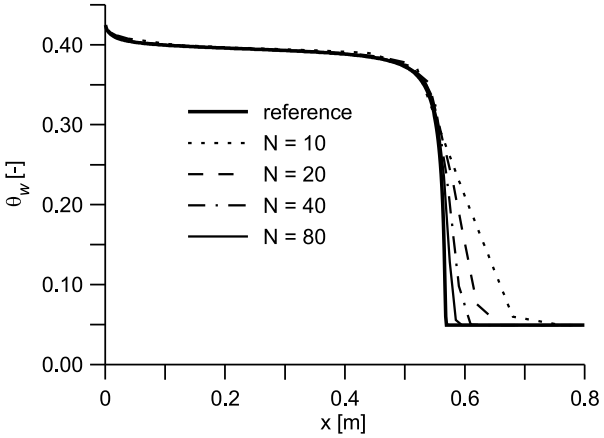

Fig. 6. Example 2: Water content profiles after 5500 s of infiltration obtained with different number of gridblocks, $\omega = 0.57$, arithmetic conductivity averaging

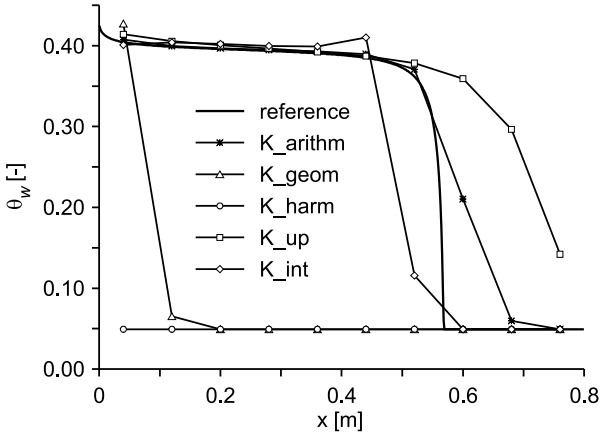

Fig. 7. Example 2: Water content profiles after 5500 s of infiltration obtained with different methods of conductivity averaging, $\omega = 0.57$, $N = 10$

the examples presented here. It shows that the choices which seem "optimal" for a given soil type and boundary conditions may lead to unsatisfactory results in other cases. Overall, the results obtained in this paper for the simulations of air and water flow are similar to the results reported by Baker (2000) and Belfort and Lehmann (2005), who analyzed the Richards equation. On the other hand, different results may be expected for other two-phase systems (e.g. water and organic liquid). Thus any general conclusions on the applicability of various averaging schemes should be very carefully formulated.

Table 5. Example 2: Numerical results for different numbers of gridblocks (N) and conductivity averaging methods

N	averaging scheme	$TMerr$ [%]	$MBerr_w$ [%]	$MBerr_n$ [%]	time steps [–]	iterations [–]	time [s]
10	arithm	8.07	4.37×10^{-03}	4.98×10^{-03}	4484	12973	2
	geom	–83.49	5.13×10^{-03}	2.36×10^{-03}	2607	7248	2
	harm	–100.00	1.07×10^{-03}	5.59×10^{-01}	370	439	0
	up	29.07	4.12×10^{-03}	4.75×10^{-03}	7472	22089	3
	int	–8.38	1.81×10^{-03}	1.90×10^{-03}	3734	10696	6
20	arithm	4.66	2.55×10^{-03}	2.85×10^{-03}	10262	30334	5
	geom	–74.63	7.04×10^{-03}	4.85×10^{-03}	6005	17472	3
	harm	–100.00	1.86×10^{-03}	5.19×10^{-01}	398	552	0
	up	17.44	2.27×10^{-03}	2.79×10^{-03}	19700	58682	10
	int	–1.62	1.33×10^{-03}	1.45×10^{-03}	9552	28176	25
40	arithm	2.46	1.41×10^{-03}	1.55×10^{-03}	24302	72476	21
	geom	–54.40	1.86×10^{-02}	1.01×10^{-02}	18589	55237	16
	harm	–100.00	2.06×10^{-03}	4.10×10^{-01}	587	1145	1
	up	10.11	1.37×10^{-03}	1.73×10^{-03}	50761	151867	43
	int	–0.31	1.15×10^{-03}	1.24×10^{-03}	23876	71161	138
80	arithm	1.15	7.80×10^{-04}	8.49×10^{-04}	57940	173413	88
	geom	–16.92	5.94×10^{-05}	9.17×10^{-05}	60627	181396	94
	harm	–100.00	2.25×10^{-03}	3.04×10^{-01}	1409	3639	2
	up	5.76	7.11×10^{-04}	9.15×10^{-04}	165233	495309	1546
	int	–0.10	5.24×10^{-04}	5.49×10^{-04}	59403	177770	652

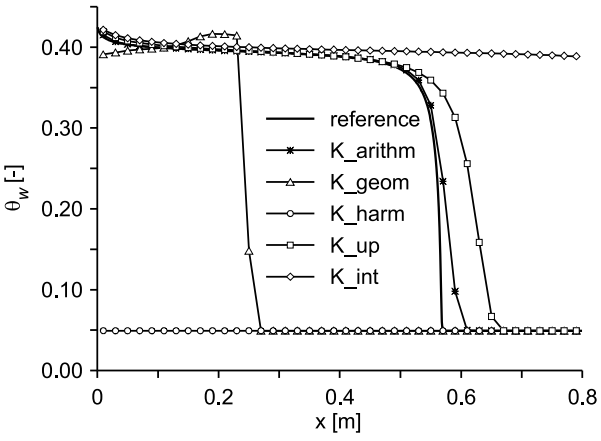

Fig. 8. Example 2: Water content profiles after 5500 s of infiltration obtained with different methods of conductivity averaging, $\omega = 0.57$, $N = 40$

5. Final Remarks

A numerical algorithm to solve 1D two-phase compressible flow in porous media was developed. The code accounts for various types of time integration schemes and conductivity averaging schemes. A series of tests has been performed to evaluate how the particular choices influence the overall efficiency and accuracy of the solution. It has been shown that using the value of the weighting parameter $\omega = 0.57$ leads to the most efficient solution with respect to the computational time. Moreover, the results demonstrated the sensitivity of the numerical solution to the choice of the conductivity averaging scheme. In the two presented examples, the arithmetic mean seem the most reliable method of averaging. However, it is difficult to draw any general conclusion on the best averaging method, since it is highly dependent on the material properties, initial-boundary conditions and spatial discretizations.

References

Baker D. L. (2000) A Darcian integral approximation to interblock hydraulic conductivity means in vertical infiltration, *Computers, Geosciences*, **26**, 581–590.

Bear J. (1972) *Dynamics of Fluids in Porous Media*, Elsevier.

Belfort B., Lehmann F. (2005) Comparison of Equivalent Conductivities for Numerical Simulation of One-Dimensional Unsaturated Flow, *Vadose Zone Journal,* **4**, 1191–1200.

Binning P. (1994) *Modelling unsaturated zone flow and contaminant transport in the air and water phases*, PhD dissertation, Department of Civil Engineering and Operations Research, Princeton University.

Binning P., Celia M. A. (1999) Practical implementation of the fractional flow approach to multi-phase flow simulation, *Advances in Water Resources,* **22**, 461–478.

Brooks R., Corey A. (1964) *Hydraulic Properties of Porous Media*, Hydrology Paper No. 3, Colorado State University, Fort Collins.

Burdine N. (1953) Relative permeability calculations from pore size distribution data, *Transactions of the American Institute of Mining, Metallurgical and Petroleum Engineers*, **198**, 71–77.

Celia M. A., Binning P. (1992) Two-phase unsaturated flow: one dimensional simulation and air phase velocities, *Water Resources Research*, **28**, 2819–2828.

Celia M. A., Boulotas E., Zarba R. (1990) A general mass-conservative numerical solution for the unsaturated flow equation, *Water Resources Research*, **26**, 1483–1496.

Chavent G., Jaffre J. (1987) *Mathematical Models and Finite Elements for Reservoir Simulation*, North-Holland, Amsterdam.

Chavent G., Jaffre J., Roberts J. E. (1997) *Generalized cell-centered finite volume methods: application to two-phase flow in porous media*, in: *Computational Science for the 21st Century*, eds. M. O. Bristau et al, Wiley, New York, 231–241.

Fučik R. (2006) *Numerical Analysis of Multiphase Porous Media Flow in Groundwater Contamination Problem,* MSc thesis, Czech Technical University in Prague, Faculty of Nuclear Sciences and Physical Engineering.

Haverkamp R., Vauclin M. (1979) A note on estimating finite diffeence interblock hydraulic conductivity values for transient unsaturated flow, *Water Resources Research*, **15**, 181–187.

Helmig R. (1997) *Multiphase Flow and Transport Processes in the Subsurface*, Springer.

Helmig R., Huber R. (1998) Comparison of Galerkin-type discretization techniques for two-phase flow in heterogeneous porous media, *Advances in Water Resources,* **21**, 697–711.

Kavetski D., Binning P., Sloan S. W. (2001) Adaptive time stepping and error control in a mass conservative numerical solution of the mixed form of Richards equation, *Advances in Water Resources*, **24**, 595–605.

Kees C. E., Miller C. T. (2002) Higher order time integration methods for two-phase flow, *Advances in Water Resources*, **25**, 159–177.

Manzini G., Ferraris S. (2004) Mass-conservative finite volume methods on 2-D unstructured grids for the Richards equation, *Advances in Water Resources*, **27**, 1199–1215.

Morton K. W. (1996) *Numerical Solution of Convection-Diffusion Problems*, Chapman, Hall.

Mualem Y. (1976) A new model for predicting the hydraulic conductivity of unsaturated porous media, *Water Resources Research*, **12**, 513–522.

Narasimhan T. N., Witherspoon P. A., Edwards A. L. (1978) Numerical model for saturated-unsaturated flow in deformable porous media: 2. Algorithm, *Water Resources Research*, **14** (2), 255–261.

Richards L. A. (1931) Capillary conduction of liquids through porous medium, *Physics*, **1**, 318–333.

Schrefler B., Xiaoyong Z. (1993) A fully coupled model for water flow and air flow in deformable porous media, *Water Resources Research*, **29**, 155–167.

Sunada D. K., McWhorter D. B. (1990) Exact integral solutions for two phase flow, *Water Resources Research*, **26**, 399–413.

Szmelter J. (1980) *Computer Methods in Mechanics*, Państwowe Wydawnictwa Naukowe, Warszawa (in Polish).

Tegnander C. (2001) Models for groundwater flow: a numerical comparison between Richards model and the fractional flow model, *Transport in Porous Media*, **43**, 213–224.

Touma J., Vauclin M. (1986) Experimental and numerical analysis of two-phase infiltration in a partially saturated soil, *Transport in Porous Media*, **1**, 27–55.

van Genuchten M. T. (1980) A closed form equation for predicting the hydraulic conductivity in soils, *Soil Science Society of America Journal,* **44**, 892–898.

Zaradny H. (1993), *Groundwater Flow in Saturated and Unsaturated Soils,* Balkema, Rotterdam/Brookfield.